J. Fluid Mech. (1979), *vol.* 97, *part* 1, *pp.* 115–127
Printed in Great Britain

Wake collapse in the thermocline and internal solitary waves

By TIMOTHY W. KAO AND HSIEN-PING PAO
Department of Civil Engineering, The Catholic University of America, Washington, D.C. 20064

(Received 28 June 1978 and in revised form 26 June 1979)

Experiments were conducted in a long channel in which a mixed region was allowed to collapse in the thermocline region of a stratified fluid. Two solitary wave-like disturbances were generated travelling to the right and left of the mixed region. The mixed region fluid was partly entrained in these waves. The waves were allowed to reflect from the end walls and to collide after the reflexions. The velocity structure of the wave was studied before, during and after a collision by means of hot-film anemometry and streak pictures. Wave speeds were accurately determined by two hot-film probes. Permanence of form and amplitude decay of the waves were observed over long distances and through successive collisions and reflexions. An analytical result for the structure of the solitary wave in an ambient stratification of the hyperbolic tangent type, but of finite total water depth, was obtained using Benney's method. Excellent agreement between the experimental and theoretical results was obtained. The results showed that the generated waves were indeed solitary waves.

1. Introduction

The collapse of a mixed region of fluid in a stratified medium has been studied extensively for the case of linear stratification. Wu (1969) found that as the mixed region spread out horizontally in space and monotonically in time, internal gravity waves were also created in the ambient fluid. In the present paper, we present the results of an experimental investigation on the collapse of a mixed region at mid-depth of a thermocline-type stratification, in which the extent of the mixed region was generally larger than the length scale of the thermocline thickness. The experiments were conducted in a long rectangular channel. The events following the collapse were quite different from those observed in a linear stratification. Two solitary wave-like disturbances were created, one propagating to the right and the other to the left. The mixed region fluid was partly entrained in these waves, which propagated unchanged for very long distances. In this paper we focus our attention on these waves. Detailed measurements were made on their propagation speed and their structure and their collisions with each other. An analytical solution was also obtained for a solitary wave in a thermocline stratification (as represented by a hyperbolic-tangent profile) for a medium of finite total depth using the method given by Benney (1966). The solution is valid within the shallow water approximation. Excellent agreement was obtained between the experimentally determined quantities and the theoretical result. The agreement confirmed the disturbances to be solitary waves obeying the Korteweg–de Vries equation.

0022–1120/80/4384–8320 $02.00

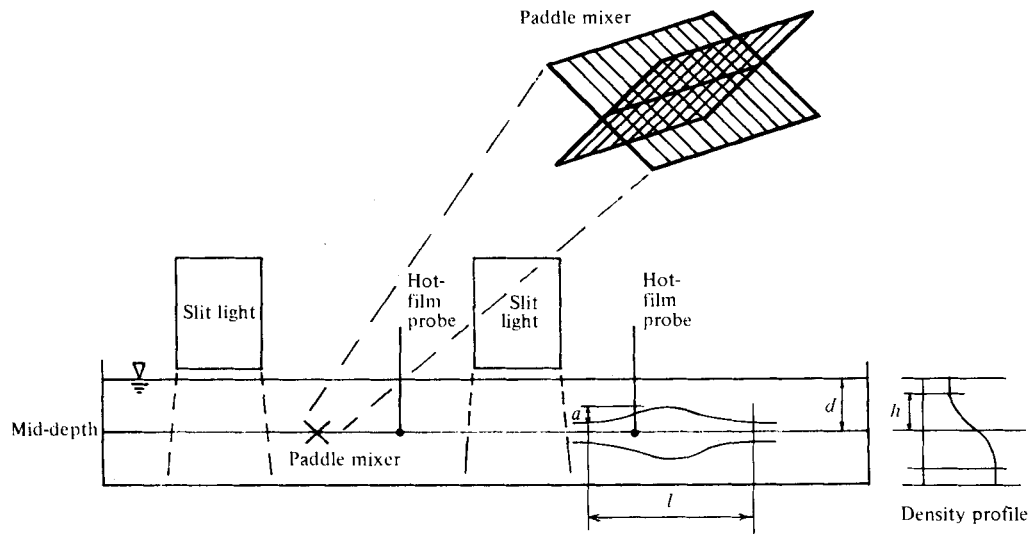

FIGURE 1. Schematic diagram showing general arrangement of the positions of the mixer, the hot-film probes and the slit-light boxes.

2. Experimental set-up and procedure

The experiments were conducted in a rectangular tank of clear acrylic sheet, 14 in. wide, 24 in. deep and 26 ft $3\frac{1}{4}$ in. long.

The mixed region was created *in situ* by using a rotary paddle mixer made of nylon fish lines tied around wire frames forming four blades. The paddle offered little resistance to the flowing fluid when stationary, but mixed the fluid efficiently when turned vigorously about its axis. The channel with the paddle in place is shown schematically in figure 1. The paddle was 3 in. in diameter and shown in detail in figure 1.

The channel was filled with a layer of salt water of density ρ_2 on the bottom and an equal depth of fresh water of density ρ_1 on the top. Before filling the fresh water layer, three thin dyed layers of intermediate density were filled by means of a floater. The total depth was usually 16 in. with the pycnocline located at the mid-depth. The fluid was then allowed to sit for half to one day for diffusion effects to create a smooth density profile. Density profiles were measured before and after each experiment by a conductivity probe. The resultant profile can be fitted by a hyperbolic-tangent profile of the form $\bar{\rho}(z) = \rho_0(1-\tilde{\omega}\tanh\alpha z)$ where $\rho_0 = (\rho_1+\rho_2)/2$, $\tilde{\omega} = (\rho_2-\rho_1)/(\rho_2+\rho_1)$ and α^{-1} is the representative half-depth of the pycnocline and z denotes the vertical co-ordinate.

The experiments were conducted in the following manner. The mixed region was first created by vigorously and rapidly rotating the paddle mixer through 260° clockwise and counter-clockwise several times. This process took place in less than four seconds. The dye in the dyed layers in the immediate vicinity of the mixer delineated, after the mixing process, the approximate extent of the mixed region. The experiment was reckoned to commence at the end of the agitation action of the mixer.

Three different measurement techniques were employed in the experiment.

(1) Direct flow visualization, by photographing the dyed layers and the dyed fluid of the mixed region.

(2) Streak-line pictures. Streak-line pictures were made using grounded Pliolite particles as tracers. These particles were almost neutrally buoyant and could even be made to achieve slightly different densities permanently by differentially heating them in water. The particles were introduced into the fluid through the free surface before the commencement of the experiment. They sank slowly (less than 0·05 in./s) to different depths of the channel. Two slit-light boxes with high-intensity light with a total slot length of 2·3 ft were placed on top of the channel (as shown in figure 1) with the opening slot located 1 in. above the water surface. The sheet of light defined a vertical plane and illuminated the Pliolite particles in the lighted plane. Streak-line pictures were taken by a Canon camera equipped with a telephoto lens and a motor drive. Tri-X (ASA 400) film was used. The camera was located 12 ft from the illuminated plane, so that the illuminated plane occupied the complete scene seen by the camera. Sequential time-exposure pictures were taken, with the room fully darkened. Time exposures of 1 s or $1\frac{1}{2}$ s were used. The streak-line pictures thus obtained represent the instantaneous flow pattern in the illuminated plane. The length of each streak could also be used to estimate instantaneous fluid velocity.

(3) Hot-film anemometry. Two hot-film anemometers (Thermosystem Model 1050) were used. The two hot-film probes were located at two different distances to the right of the centre of the mixer at mid-depth (see figure 1). The probes measured the horizontal velocity of the fluid at these locations. The output from the probes was recorded on a high-precision Sanborn strip chart recorder continuously throughout the duration of the experiment. By measuring the arrival times of the peaks of the disturbance, the wave speed could be accurately determined. The temporal (and spatial) velocity structure at mid-depth and the flow behaviour during collision were measured quantitatively. Temporal decay of the amplitude was also recorded.

3. Experimental and theoretical results and discussion

The following sequence of events was observed in a typical experiment. A mixed region approximately delineated by the entrained dye was formed by the mixer. The mixed region started to collapse at the commencement of the experiment. As it collapsed, two solitary wave-like vertically symmetric bulges were observed with the indication that the fluid of the mixed region occupied the core of each bulge. One travelled to the right and the other to the left of the mixer. Both bulges were able to travel without change in form. They were reflected, without change in form, from the end walls of the channel and collided head-on at the conjugate point (i.e. the location at the same distance from the right end wall as that of the mixer from the left end wall). During collision the two bulges appeared to superpose, resulting in apparent doubling of the amplitude of the bulge. The individual bulges re-emerged again without change in form after the collision. These features suggest strongly that the disturbances resulting from wake collapse in the thermocline are solitary waves similar to those observed by Davis & Acrivos (1967). A typical solitary wave is shown in figure 2 (plate 1). The grid at the back consists of 1 in. squares. Figure 2(*a*) shows the wave immediately after its formation travelling to the right. Figure 2(*b*) shows the same wave at a later time. As the wave travelled over long distances, its amplitude gradually

attenuated due to viscosity and its wavelength gradually increased. The form, however, remained similar. Towards the final stages, the amplitude became unobservably small. However, the hot-film record of the horizontal velocity at mid-depth continued to delineate the typical signal of the wave with a well-defined peak. Because of this feature, the wave speed of the infinitesimal-amplitude wave was accurately measurable.

Before presenting the main experimental results, their details, and their interpretation, let us investigate first, from a theoretical view-point, the features of a solitary wave in a thermocline-type stratification of finite total depth.

3.1. *Theoretical consideration*

A number of theoretical works have been published on internal solitary waves in a continuously stratified fluid, principally by Benney (1966), Benjamin (1966, 1967), Davis & Acrivos (1967), and Ono (1975). Benjamin (1967) considered a hyperbolic tangent density profile for a medium of infinite total depth and Davis & Acrivos (1967) considered a similar three-layered stratification of infinite total depth.

If a denotes the wave amplitude, l the wave length and d the undisturbed half-depth of the fluid (see figure 1), two important dimensionless length ratios can be formed, namely, an amplitude parameter, $\epsilon = a/d$, and a wavelength parameter, $\mu = d/l$. Benney's (1966) method is to expand the stream function and density fields in terms of ϵ and μ^2 and develop asymptotic solutions in the neighbourhood of $\epsilon = \mu^2 = 0$ with $\epsilon/\mu^2 = 1$ (i.e. $al^2 = d^3$). The theory is thus a 'shallow-water' theory. It is also well known that $\epsilon/\mu^2 = 1$ represents the condition that the large-amplitude breaking tendency is balanced by dispersion (see Ursell 1953 and Benney 1966). This balance allows the existence of the solitary wave of the Korteweg–de Vries (KdV) type with a sech^2 wave form. In the theory of Benjamin (1967) and Ono (1975), the total depth of the fluid is infinite. The fluid is, however, divided into two regions, one of half-depth h in which the density varies continuously with height, and an outer one, extending to infinity, in which the density is constant. [For the hyperbolic-tangent profile h is not precisely defined as pointed out by Benjamin (1967). In any case, h is several times larger than α^{-1}, the 'representative half-depth' of the thermocline. This point is not really important in the following development but should be noted.] The amplitude and wavelength parameters are now defined as $\epsilon' = a/h$ and $\mu' = h/l$. These authors then showed that another kind of solitary wave exists in the neighbourhood of $\epsilon' = \mu' = 0$ with $\epsilon'/\mu' = 1$ (i.e. $al = h^2$). This solitary wave is governed by an equation different from the KdV equation (an equation popularly known as the Benjamin–Ono equation), and has a wave form which is described by a Lorentzian distribution.

In this section, we apply Benney's method to the study of the solitary wave in a fluid of limited total depth with a hyperbolic-tangent density profile (or thermocline profile). The thermocline region is located at mid-depth. The theoretical development of the method is found in Benney (1966) and will not be repeated in detail here. We denote the horizontal and vertical and time co-ordinates by x, z and t and introduce dimensionless quantities $\tilde{x} = x/l$, $\tilde{z} = z/d$, $\tilde{t} = (U/l)t$ where $U = (gd)^{\frac{1}{2}}$. The non-dimensional stream function is then written as

$$\psi(\tilde{x}, \tilde{z}, \tilde{t}) = A\phi^{(0,0)}(\tilde{z}) + \epsilon A^2\phi^{(1,0)}(\tilde{z}) + \mu^2 A_{\tilde{x}\tilde{x}}\phi^{(0,1)}(\tilde{z}) + \ldots, \tag{1}$$

where the superscripts (i,j) are associated with the orders of ϵ and μ^2 respectively, the subscripts denote differentiation, and A is given by

$$A_{\tilde{t}} = -\tilde{c}_0 A_{\tilde{x}} + \epsilon 2rAA_{\tilde{x}} + \mu^2 s A_{\tilde{x}\tilde{x}\tilde{x}} + \ldots \tag{2}$$

in which $\tilde{c}_0 = c_0/U$, with c_0 denoting the dimensional zeroth order wave speed, and s and r are constants determinable from the zeroth-order solution. To the first order, with $\epsilon = \mu^2$, (2) is the well-known Korteweg–de Vries equation which governs the evolution of an initial disturbance. This equation has a solitary wave solution propagating in one direction:

$$A(\tilde{x},\tilde{t}) = a_m \operatorname{sech}^2 b[\tilde{x} - (\tilde{c}_0 + \epsilon\tilde{c}')\tilde{t}], \tag{3}$$

where $a_m = 6sb^2/r$, $\tilde{c}' = -4sb^2$. The solution for $\phi^{(0,0)}(z)$ can in turn be found from the zeroth-order eigenvalue problem given in dimensional co-ordinates by

$$(\bar{\rho}\phi_z^{(0,0)})_z - (g\bar{\rho}_z/c_0^2)\phi^{(0,0)} = 0; \quad \phi^{(0,0)}(0) = \phi^{(0,0)}(d) = 0, \tag{4}$$

for stratified fluid between rigid boundaries $(-d,d)$ with a plane of symmetry about $z = 0$. For the stratification given by

$$\bar{\rho}(z) = \rho_0(1 - \tilde{\omega}\tanh\alpha z) \tag{5}$$

and with the Boussinesq approximation, the eigenvalue problem given in (4) becomes

$$\phi_{zz} + \left(\frac{g\tilde{\omega}\alpha\operatorname{sech}^2\alpha z}{c_0^2}\right)\phi = 0, \tag{6}$$

$$\phi(0) = \phi(d) = 0, \tag{6a}$$

the superscripts $(0,0)$ being dropped for the sake of simplicity. Equation (6) is now to be solved subject to the boundary condition (6*a*).

Equation (6) may be readily transformed into Legendre's equation by using $\eta = \tanh\alpha z$ as the independent variable (see Krauss 1966, pp. 35–38; also Benjamin 1967) to give

$$\frac{d}{d\eta}\left[(1-\eta^2)\frac{d\phi}{d\eta}\right] + p(p+1)\phi = 0, \tag{7}$$

where we have set $(g\tilde{\omega}/\alpha c_0)$ to be $p(p+1)$ with $p > 0$ but *not* an integer. Equation (7) is solved subject to the boundary conditions

$$\phi(0) = \phi(\tanh\alpha d) = 0. \tag{7a}$$

The case for infinite depth has been investigated by Benjamin (1967). For that case $\tanh\infty = 1$ and p is then an odd integer n, of which $n = 1$ is the one of greatest interest. For most experimental work αd is $O(10)$ or less. We thus seek a solution to (7) and (7*a*) by expanding the eigenvalue p around the odd integers. For the lowest mode we set

$$p = 1 + \delta + \delta^2 + \ldots, \tag{8}$$

where $\delta \sim O(10^{-1})$. The solution to (7) satisfying the condition $\phi(0) = 0$ is the Legendre function of order p:

$$L_p(\eta) = \eta + \sum_{k=1}^{\infty} B_k \eta^{2k+1} \tag{9}$$

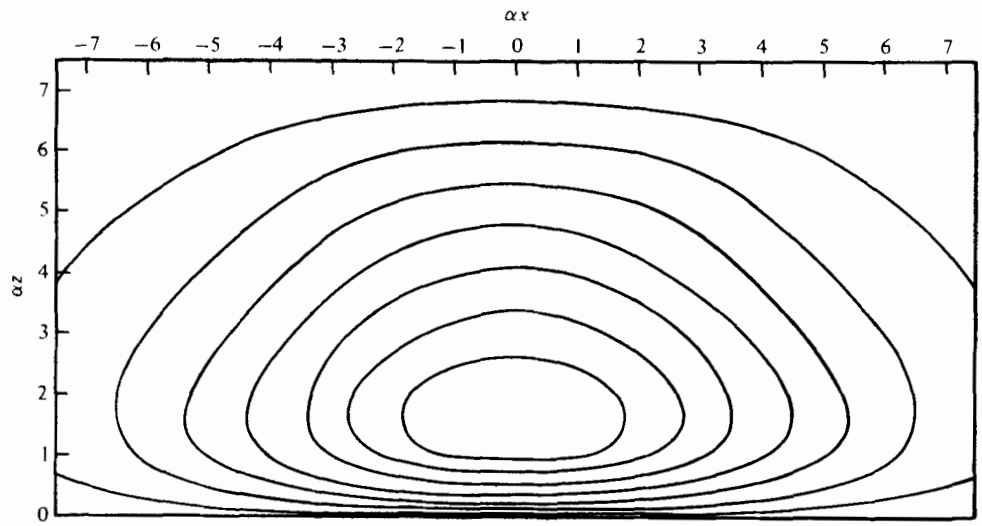

FIGURE 3. Theoretical instantaneous streamline pattern above the plane of symmetry.

where

$$B_k = \frac{(-1)^k}{(2k+1)!}[(p-1)(p-3)\dots(p-2k+1)][(p+2)(p+4)\dots(p+2k)].$$

For the lowest mode, on substitution of (8) into (9), we have to the first order in δ the solution

$$\phi(\eta) \simeq \eta + \delta \sum_{k=1}^{\infty} \frac{1}{2k}(-\eta)^{2k+1}.$$

The above series converges for $|\eta| < 1$ but extremely slowly. However, it is comforting to find that the series has a closed form representation, i.e.

$$\phi(\eta) \simeq \eta + \tfrac{1}{2}\delta\eta[\ln(1-\eta^2)]. \tag{10}$$

The second boundary condition, $\phi(\tanh \alpha d) = 0$, now gives

$$\delta = [\ln(\cosh \alpha d)]^{-1}. \tag{11}$$

For $\alpha d = 7{\cdot}5$, for example, $\delta = 0{\cdot}147$.

In a frame of reference such that the origin, $x = 0$, coincides with the peak location instantaneously, the first-order solution for ψ is now, up to a multiplicative constant $\tilde{\epsilon}$,

$$\psi = \tanh \alpha z \left[1 - \frac{\ln(\cosh \alpha z)}{\ln(\cosh \alpha d)}\right] \operatorname{sech}^2 b' \alpha x, \tag{12}$$

where $b' = (be^{\frac{1}{2}}/\alpha d)$ and $\tilde{\epsilon} = \epsilon a_m$. The instantaneous streamline pattern given by (12) is shown in figure 3 for $\alpha d = 7{\cdot}5$ with b' arbitrarily chosen to be $\frac{1}{5}$. Only the part above the plane of symmetry is shown in figure 3.

From the relation $a_m = 6sb^2/r$ given earlier, we see that $b' = (\tilde{\epsilon}r/6s)^{\frac{1}{2}}(\alpha d)^{-1}$ or

$$\tilde{\epsilon} = 6s(\alpha d)^2 (b')^2/r. \tag{13}$$

αd	$r/(\alpha d)$	r	$s(\alpha d)^2/\tilde{c}_0$	$s/\tilde{c}_0$
7·5	−0·4956	−3·72	−1·4613	−0·0260
12	−0·5360	−6·43	−2·5590	−0·0178
16	−0·5523	−8·84	−3·5623	−0·0139

TABLE 1. Values of the theoretical constants r and s for given (αd).

The constants r and s are determined from the zeroth-order eigenfunction ϕ by the formulae

$$r = -\frac{3}{4}\frac{\int_0^1 \phi_{\tilde{z}}^3 d\tilde{z}}{\int_0^1 \phi_{\tilde{z}}^2 d\tilde{z}}, \quad s = -\frac{\tilde{c}_0}{2}\frac{\int_0^1 \phi^2 d\tilde{z}}{\int_0^1 \phi_{\tilde{z}}^2 d\tilde{z}}, \tag{14}$$

within the Boussinesq approximation. We note that r and s depend on the value of αd. Values of r and $s/\tilde{c}_0$ are tabulated for selected values of αd in table 1. The maximum dimensional horizontal velocity $u_{\max}$ associated with the wave occurs at $z = 0$ under the peak. Therefore, on differentiating the streamfunction with respect to $\tilde{z}$ and setting $\tilde{x} = \tilde{z} = 0$, we obtain

$$u_{\max}/c_0 = (\alpha d)\,\tilde{\epsilon}/\tilde{c}_0. \tag{15}$$

The zeroth-order wave speed c_0 is given by

$$c_0^2 = \left[\frac{g\tilde{\omega}}{(2+3\delta)\,\alpha}\right]. \tag{16}$$

From (3), the dimensionless first-order wave speed, $\tilde{c}$, is $\tilde{c} = \tilde{c}_0 + \epsilon\tilde{c}'$. From this, on using the relations for a_m and $\tilde{c}'$ immediately following (3), it is seen that

$$\Delta c/c_0 = -\tfrac{2}{3}r\tilde{\epsilon}/\tilde{c}_0, \tag{17}$$

where $\Delta c/c_0 \equiv (c-c_0)/c_0 = (\tilde{c}-\tilde{c}_0)/\tilde{c}_0$. From (15) and (17), we get, upon elimination of $\tilde{\epsilon}/\tilde{c}_0$,

$$\frac{\Delta c}{c_0} = -\frac{2}{3}\frac{r}{(\alpha d)}\frac{u_{\max}}{c_0}. \tag{18}$$

Values of $r/(\alpha d)$ for $7{\cdot}5 < \alpha d < 16$ are shown in table 1. These values do not vary substantially in that range, so that in that range (18) becomes

$$\Delta c/c_0 = 0{\cdot}35u_{\max}/c_0. \tag{18a}$$

Equation 18 gives the increase of wave speed Δc due to the nonlinear effect of large amplitude as manifested by $u_{\max}$. For later experimental comparison, $u_{\max}$ is a better measure of the amplitude than the displacement amplitude of the isopycnic, since the latter is not readily measurable and varies as a function of the depth, decreasing to zero at the upper and lower boundaries.

It should be noted that the theory contains the parameter (αd). Caution should be exercised in applying the present results when (αd) is large and α finite. Indeed, for the present results to be applicable, $\mu^2 = (d/l)^2$ must remain small, i.e. $O(10^{-1})$. The wavelength l of the solitary wave, to be sure, is not definite, but we may follow Lamb (1932) and take l to be the length spanned by the wave between the locations where

the amplitude is one-tenth of its maximum. For the sech^2 wave form given in (12) the amplitude is one-tenth when the argument is 1·818. Thus l is given by $b'\alpha l = 3{\cdot}636$ (i.e. $\alpha l = 3{\cdot}636/b'$) whence

$$\mu^2 = (\alpha d)^2 (b'/3{\cdot}636)^2. \tag{19}$$

Therefore, for a given αd and an experimentally determined value of b', the theory is applicable if μ^2 is $\sim O(10^{-1})$.

3.2. *Experimental results and discussion*

A series of experiments was run for $6{\cdot}9 < \alpha d < 17$ with $1{\cdot}15 > \alpha^{-1} > 0{\cdot}45$ in. and $\tilde{\omega} = 0{\cdot}01$. The instantaneous streamline pattern of the wave was obtained by streak-line photography. The speed of the wave as well as its temporal structure was measured by two hot-film probes at two horizontal locations at mid-depth. These probes also measured the horizontal velocity at these locations. In this section, the experimental results are presented and compared with the theory of the previous section. The agreement between the experimental and theoretical results confirms that the disturbances are solitary waves obeying the Korteweg–de Vries equation, in the range of parameters tested.

Figure 4(*a*) (plate 2) depicts a wave travelling to the left in a typical experiment ($\alpha d = 7{\cdot}5$, $\alpha^{-1} = 1$ in., $\tilde{\omega} = 0{\cdot}01$). Figure 4(*b*) shows the instantaneous flow pattern of the streak-line picture of the same wave; the time exposure was one second. The picture shows two closed circulation patterns symmetrically located above and below the mid-depth of the fluid. The fluid velocity is horizontal at mid-depth and has a maximum value there as seen from the length of the streaks. These qualitative features are in agreement with the theoretical findings of the previous section. A closer comparison of the theoretical and experimental instantaneous streamline pattern for the same conditions is shown in figure 4(*c*) (plate 3). (The theoretical pattern is the same one as in figure 3 with $\alpha d = 7{\cdot}5, b' = \frac{1}{5}$.) The streak-line picture was taken at 84 seconds after the commencement of the experiment. At that time the value of b' was determined to be $\frac{1}{5}$. (The experimental determination of b' will be discussed presently.) The corresponding wavelength l, calculated from the formula $\alpha l = 3{\cdot}636/b'$, was then equal to 18·2 in. The horizontal scale in figure 4(*c*) indicates distances in 1 inch intervals. The point $x = 0$ indicates the instantaneous horizontal location of the peak of the wave. It is seen from this figure that the agreement is very good indeed. By measuring the lengths of the streaks, it is seen that the ratio of horizontal velocity in the upper portion to the maximum velocity $u_{\max}$ at mid-depth is approximately 0·15 at $x = 0$. This is in good agreement with the theoretical ratio which can be easily shown to be equal to δ at $x = 0$. For this experiment with $\alpha d = 7{\cdot}5$, δ is 0·147 from (11).

The path of the solitons after their generations is shown schematically in the x–t plot of figure 5 where the locations of the probes are also indicated. The two solitons emerge at $t = 0$, reflect, and collide successively as time progresses. Possible time delays (or phase shifts) during collisions are omitted in this schematic diagram. We denote the soliton travelling to the right when it emerged by R and the one to the left by L. The points of collision are expected to be located approximately at the mixer and its conjugate point. An actual representative experimental realization is shown in figure 6 where the raw data from the hot-film output is inserted in the x–t diagram. For this run, the mixer was placed 106 in. from the left end wall. The first

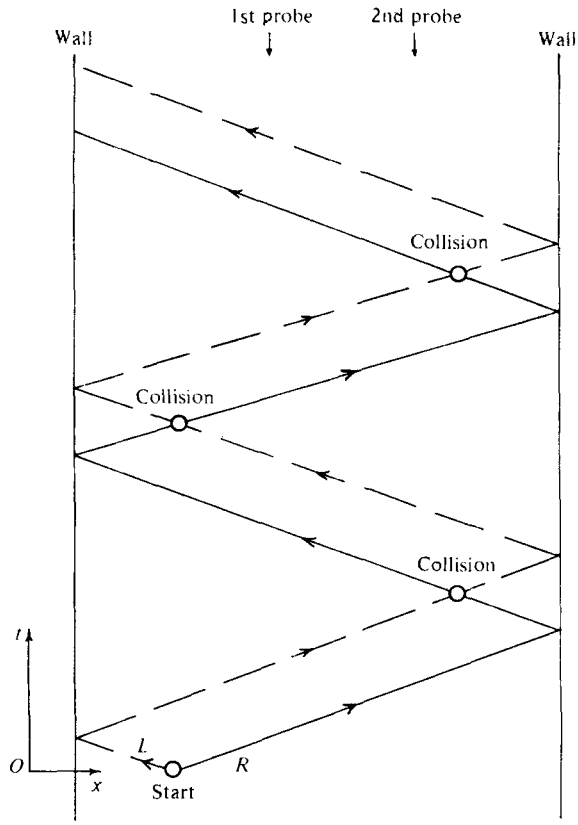

FIGURE 5. Schematic path of the two solitons after their generation in the x–t plot. The dotted line indicates the path of the soliton L and the solid line the soliton R.

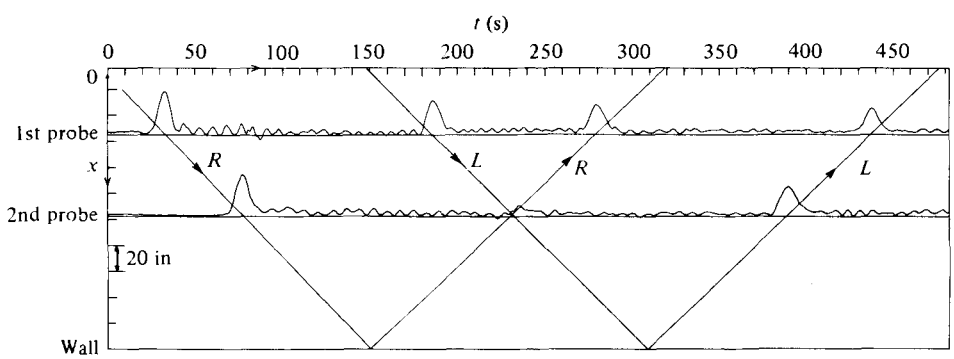

FIGURE 6. A realization of the velocity record from two hot-film probes, displayed in the x–t plot, for the same experiment as shown in figure 4. t is measured from the commencement of the experiment and x is measured from the centre of the mixer. See text for a detailed description. The second probe is near the collision point.

probe and second probe were at 44⅜ in. and 107 in. respectively to the right of the mixer, which placed the second point at 102¼ in. from the right end wall so that the second probe was close to the conjugate point.

The arrival of the soliton R directly after its generation at the first probe and then the second probe is clearly seen in figure 6. It is also seen that the solitons are followed

by a train of internal waves of small amplitude with a rather narrow frequency band centred around a period of about 7 s. (The internal waves are difficult to see visually.) These manifestations are typical of the solution of the Korteweg–de Vries equation for an initial disturbance. The speed of soliton R, determined precisely by the arrival time of the peak and the distance travelled, was found to be 1·39 in./s. The soliton L arrived at the first probe after reflexion from the left end wall in 186 s, travelling a total distance of 256·4 in. giving a speed of 1·36 in./s. The most interesting feature occurred at the second probe when soliton L, going to the right, collided head-on with the soliton R, moving towards the left after reflecting from the right end wall. The hot-film trace from the second probe shows that during the period of interaction the horizontal velocity is essentially annihilated. The small residual velocity is due to the fact that the probe was not exactly at the collision point. As shown in the trace for the first probe, the soliton R re-emerged after the collision as the third bump, at $t = 280$ s, having travelled a total distance of 374 in. The last bump on the trace of the second probe is the re-emerged L soliton which had travelled a distance of $523\frac{1}{2}$ in. in 290 s. The speeds of the emergent waves were both 1·34 in./s. The peak amplitudes of the waves were attenuated somewhat. The experiment was continued for over 13 minutes beyond the record.

A number of such experiments was run with complete records of the hot-film signals. The hot-film signals were first analysed for the horizontal velocity structure. A typical record (raw data) of a soliton wave form on an expanded time scale (1 s = 5 divisions) is shown in figure 7 (plate 3) for $\alpha d = 6{\cdot}96$. If t_m denotes the time of arrival of the peak, we can construct the curve for the normalized horizontal velocity $u/u_{\max}$ as a function of a dimensionless time scale given by $1{\cdot}2(t-t_m)/(t_0-t_m)$, where t_0 is the time when $u/u_{\max}$ is 0·305. This choice of the constants is made since we anticipate the curve to follow a sech^2 profile and since $\operatorname{sech}^2(1{\cdot}2) = 0{\cdot}305$. We may proceed one step further. The temporal structure can be converted into a spatial structure in a co-ordinate moving with the local wave speed c by setting $x = c(t-t_m)$, since the wave speed is a constant during the time of transit of the wave over a fixed probe. Thus we write $1{\cdot}2(t-t_m)/(t_0-t_m) = 1{\cdot}2x/x_0 = 1{\cdot}2(\alpha x)/(\alpha x_0)$, where x_0 is now the spatial distance in which the amplitude of the wave drops to 0·305 of the maximum value. We also identify $1{\cdot}2/(\alpha x_0)$ with b' in (12). A large number of such wave forms were analysed. The normalized velocity structure is shown in figure (8) where $u/u_{\max}$ is plotted against $(b'\alpha x)$. The solid curve is the curve $u/u_{\max} = \operatorname{sech}^2(b'\alpha x)$. It is seen that the data agree with the sech^2 curve to a remarkable degree of precision. Note that only the rising portions of the hot-film signals were used in the analysis. The full wave was slightly asymmetric towards the tail of the falling portion as can be seen in figure (7). For each value of α in the various experiments, b' is determined by the formula $b' = 1{\cdot}2/(\alpha x_0)$. It should be noted that the data plot in figure 8 is independent of α. The determination of b' is of course dependent on α. It was also found that, for the same experiment, b' became smaller (i.e. the wavelength became larger) as the wave amplitude decreased.

The agreement of the data with the sech^2 curve in figure 8 indicates that the KdV-type solution presented herein is valid for the range of parameters tested. To make sure that the shallow-water assumption was satisfied, we compute μ^2 using (19). This is shown in table 2 for representative values of b' found in the range of values of αd tested. Table 2 shows that the values of μ^2 are indeed of $O(10^{-1})$ as required by the

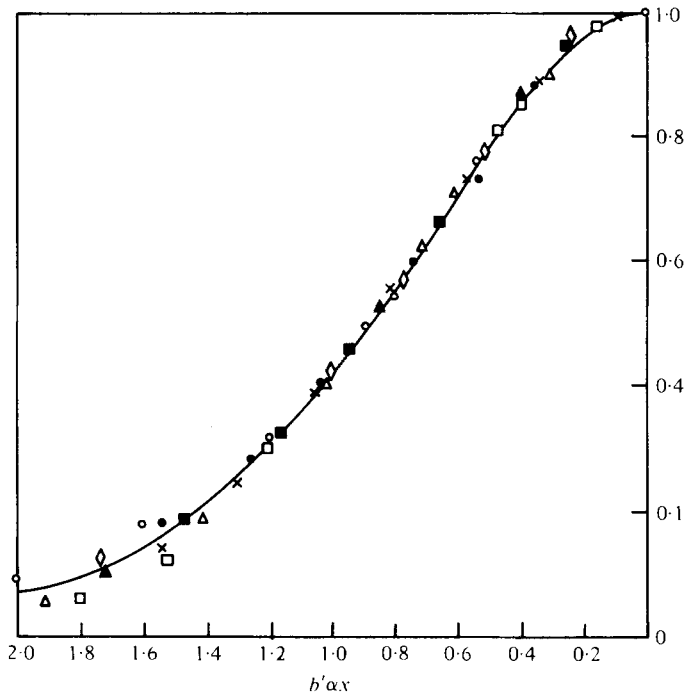

FIGURE 8. Normalized spatial velocity structure at mid-depth ($z = 0$) where u/u_{max} is plotted against $b'\alpha x$. The solid curve is the curve $u/u_{max} = \text{sech}^2(b'\alpha x)$. Each symbol represents a different value of αd ($7 < \alpha d < 16$).

αd	b'	μ^2
6·95	0·20	0·146
7·5	0·20	0·170
8	0·18	0·157
8	0·19	0·175
15·4	0·07	0·088
15·4	0·186	0·620
16	0·14	0·379
16	0·13	0·327

TABLE 2. Experimental values of μ^2.

theory. Furthermore, these values indicate, *a posteriori*, that the way the wavelength is defined is an appropriate measure of the length scale l.

As mentioned at the beginning of § 3, the wave speed of the wave when the amplitude became unobservably small visually could still be accurately determined by the hot-film signal in the final stages of decay. This furnishes us a means of determining c_0. The values of c_0 obtained for several experiments, all with $\tilde{\omega} = 0{\cdot}01$, are listed on table 3. These are compared with the theoretical values as calculated by using (16). The values of δ calculated from (11) are also listed. The values of α^{-1} used were determined by the salinity probe at the end of the experiment. The agreement between the experiment and the theory is found to be excellent. Such an agreement is a necessary

α^{-1}	αd	δ	c_0 (equation 16)	c_0 (measured)
1·15 in.	6·9	0·160	1·34 in./s	1·34 in./s
1·00 in.	7·5	0·147	1·26 in./s	1·26 in./s
0·76 in.	10·5	0·102	1·12 in./s	1·10 in./s
0·52 in.	15·4	0·068	0·96 in./s	0·98 in./s

TABLE 3. Experimental values of c_0.

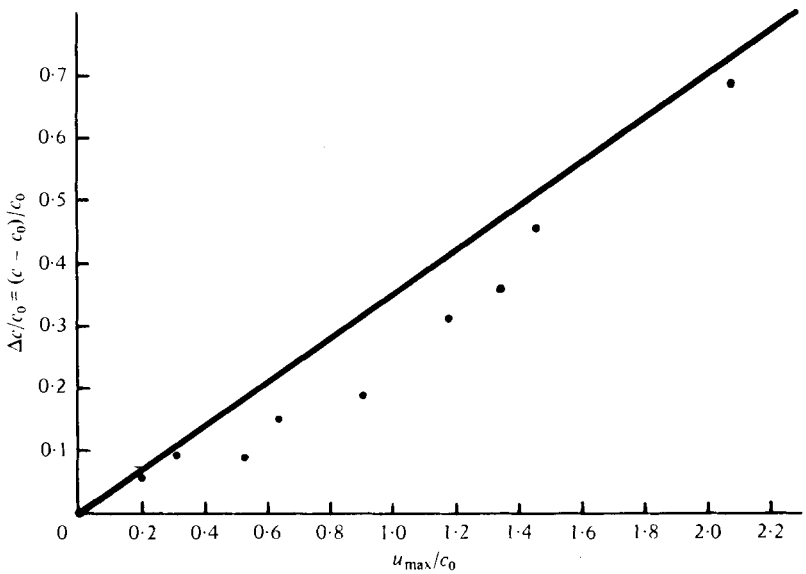

FIGURE 9. Dependence of wave speed increment $\Delta c/c_0$ on u_{max}/c_0. The solid line is the theoretical result.

check on the experiments since the formula for c_0 as given by (16) is independent of the restrictions on the nonlinear theory and is unquestionably valid for the range of αd explored. It should be noted that due to the collapse of the mixed region, the value of α^{-1} at the end of the run was larger than that at the beginning of the experiment by about 15% in most runs. This increase is also an indication of the change in potential energy between the beginning and end of the experiment. The change in potential energy, in turn, is a measure of the energy input of the stirring process for the creation of the mixed region. It was observed that more vigorous stirring produced larger amplitude solitons and larger increases in α^{-1} at the end of the experiment.

A final comparison with the theory is obtained by plotting the increment of wave speed $(c-c_0)/c_0 (\equiv \Delta c/c_0)$ against u_{max}/c_0. This is shown in figure 9. The solid line is the theoretical result given by (18*a*). The experimental data were from an experiment with average $\alpha d = 16$. The large-amplitude results were obtained at the beginning of the experiment, and the small-amplitude results were towards the final stages of the experiment. The values of c_0 for the initial and final stages were thus calculated from (16), based on the values of α measured before and after the experiment respectively, and an intermediate value was used for the intermediate points. It is seen from figure 9 that the agreement is satisfactory in general and very good for smaller

values of the amplitude $u_{\max}/c_0$. Since the absolute values of $u_{\max}$ were involved in this plot, the presence of any hot-film anemometry errors became pronounced.

We now turn briefly to the question of whether there was any phase shift during a head-on collision, or equivalently, a reflexion from the end wall. A typical visual collision sequence is shown in figure 10 (plate 4). Picture (*a*) was taken at approximately 6 s before collision, (*b*) at approximately mid-collision and (*c*) approximately 9 s after collision. It is seen that the form of the solitary waves was well preserved after undergoing the collision. The timing of the clock and the lack of definition of the exact locations of the peaks precluded any conclusions being drawn on phase changes. To obtain more quantitative information, experiments were conducted with the two hot-film probes placed at 30 in. and 20 in. from one end wall so that the time of arrival of the peak at these two locations before and after its collision with the wall can be accurately determined to within one-twentieth of a second. From these arrivals the wave speed before and after the collision was found. The temporal phase shift was then obtained. The results yielded a negative phase shift of one to two seconds with a considerable degree of uncertainty. The uncertainty was mainly due to the effect of the end wall on the wave speed. The reflected wave wave speed was further complicated by the interaction with the dispersive tail of the incoming wave. In view of these uncertainties, no correlation of the phase shift with amplitude was possible. Nevertheless, the overall effect of the reflexion process appeared to be a hesitation of the wave at the end wall.

The authors are indebted to Mr Y. J. Lin for his part in performing the experiments. The work is partially supported by the National Science Foundation under grants ATM-75-08408 and ENG-77-01496.

REFERENCES

BENJAMIN, T. B. 1966 Internal waves of finite amplitude and permanent form. *J. Fluid Mech.* **25**, 241.

BENJAMIN, T. B. 1967 Internal waves of permanent form in fluids of great depths. *J. Fluid Mech.* **29**, 559.

BENNEY, D. J. 1966 Long non-linear waves in fluid flows. *J. Math. & Phys.* **45**, 52.

DAVIS, R. E. & ACRIVOS, A. 1967 Solitary internal waves in deep water. *J. Fluid Mech.* **29**, 593.

KRAUSS, W. 1966 *Methoden und Ergebnisse der Theoretischen Ozeanographie.* II. *Interne Wellen.* Berlin: Gebruder Borntraeger.

LAMB, H. 1932 *Hydrodynamics*, art. 252. Dover.

ONO, H. 1975 Algebraic solitary waves in stratified fluids. *J. Phys. Soc. Japan* **39**, 1082.

URSELL, F. 1953 The long wave paradox in the theory of gravity wave. *Proc. Camb. Phil. Soc.* **49**, 685.

WU, J. 1969 Mixed region collapse with internal wave generation in a density-stratified medium. *J. Fluid Mech.* **35**, 531.

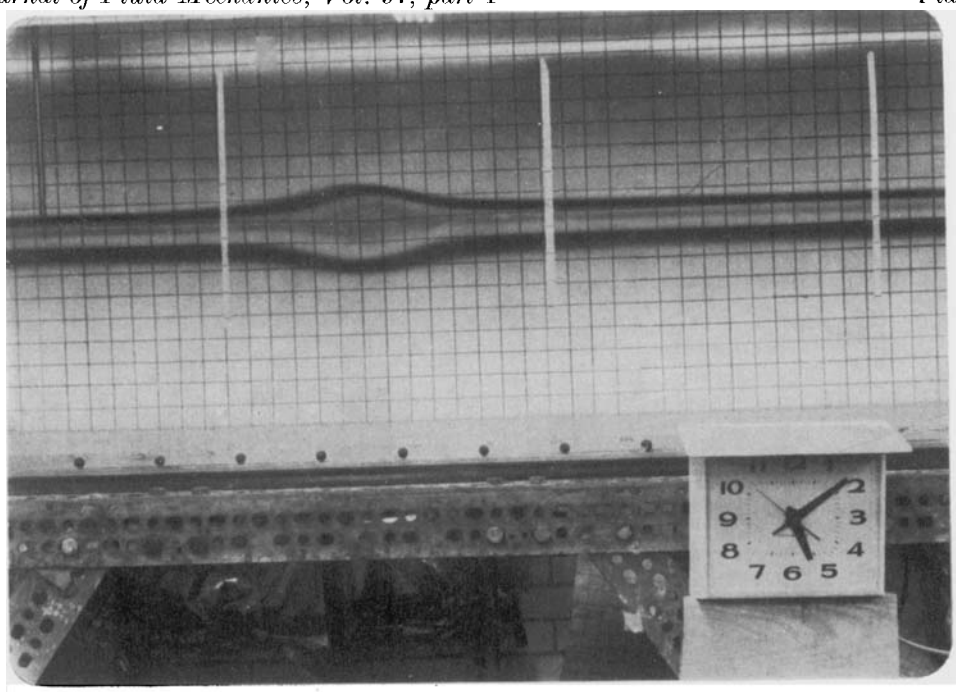

(*a*)

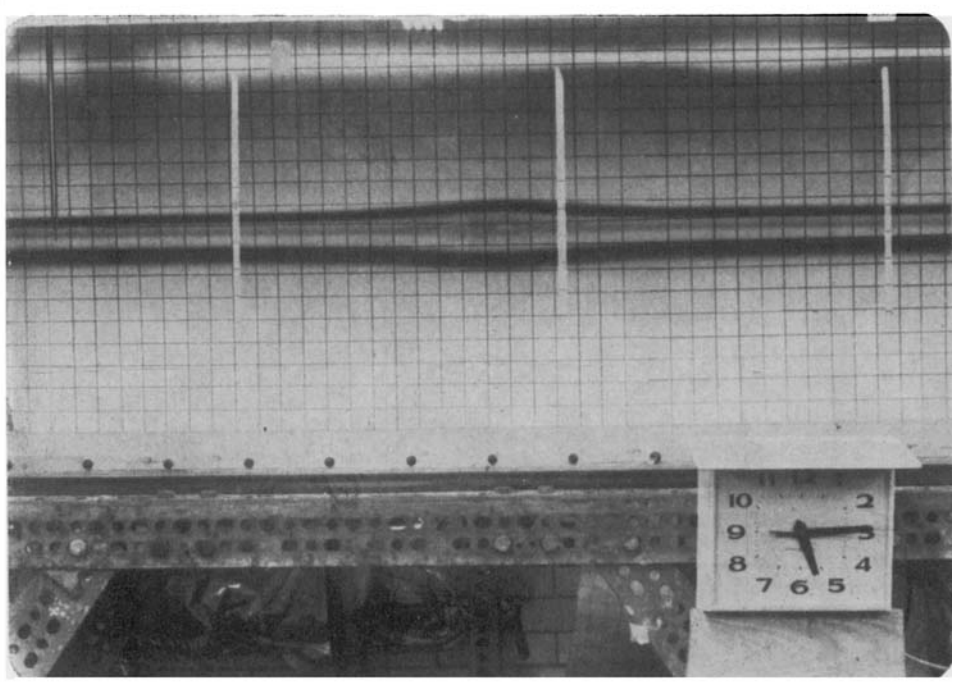

(*b*)

FIGURE 2. (*a*) A typical solitary wave soon after its formation. The grid in the back has a 1 in. spacing. (*b*) The same wave at a later time.

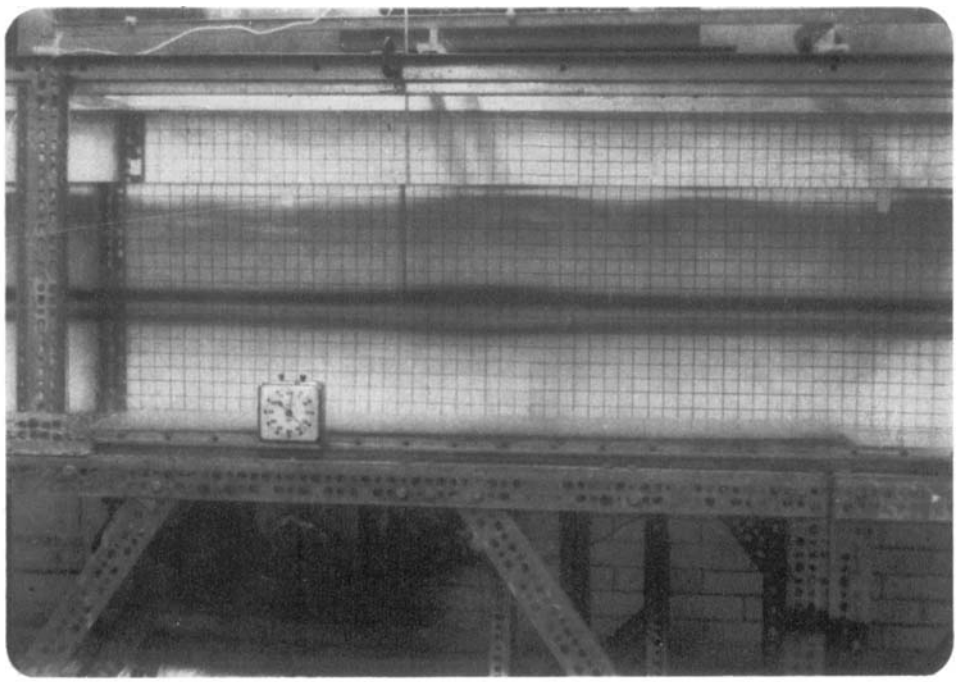

(*a*)

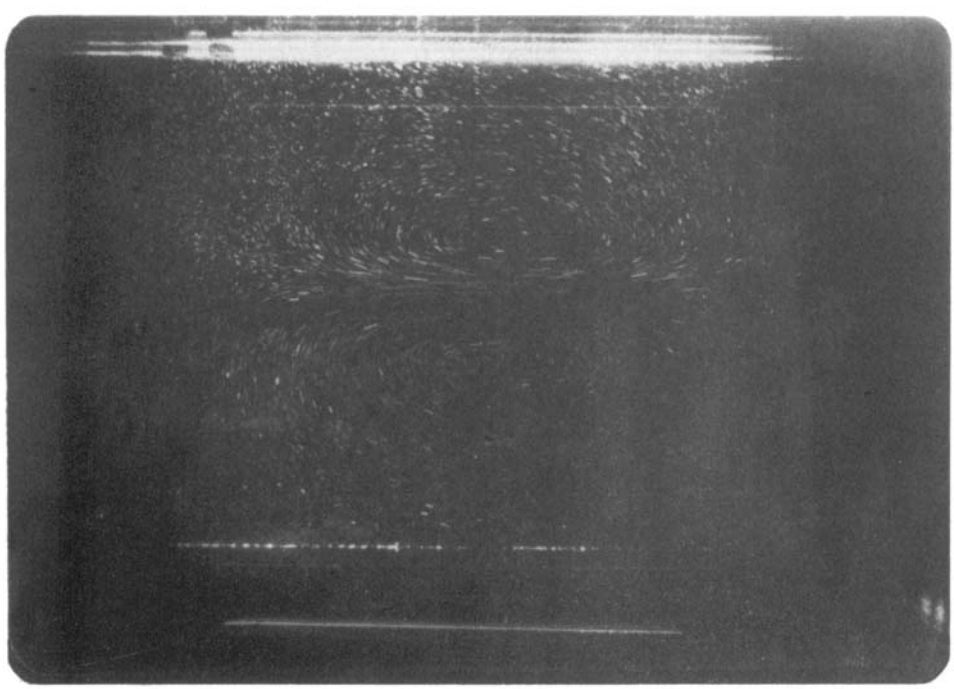

(*b*)

FIGURE 4 (*a*, *b*). For legend see facing page.

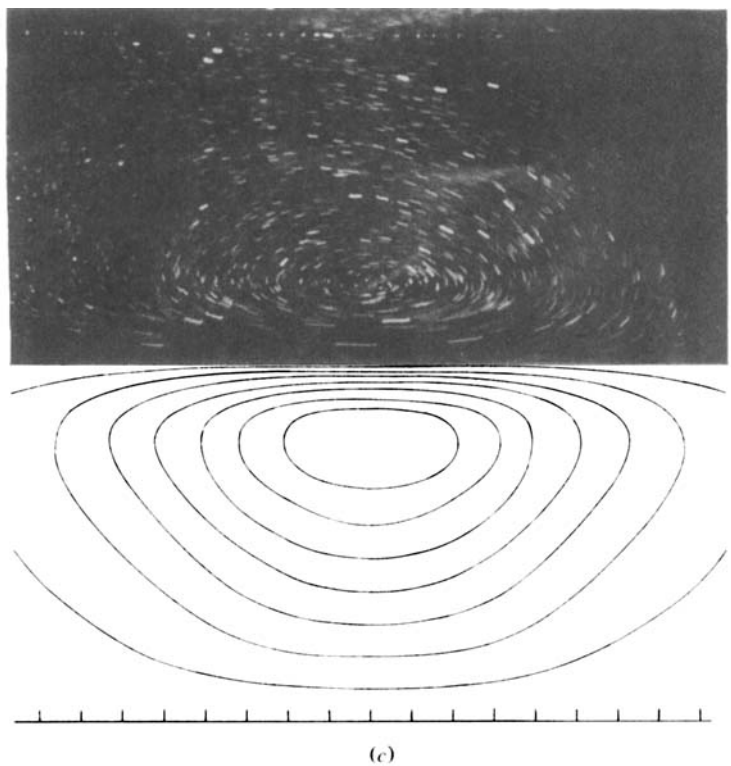

(*c*)

FIGURE 4. (*a*) Visual view of a solitary wave travelling to the left at 82·5 s after the commencement of the experiment. $\tilde{\omega} = 0{\cdot}01$, $\alpha^{-1} = 1$ in. (*b*) The streak-line picture of the same wave at approximately the same time. (*c*) Comparison of experimental and theoretical instantaneous stream-line patterns. The lower part is the theoretical pattern of figure 3.

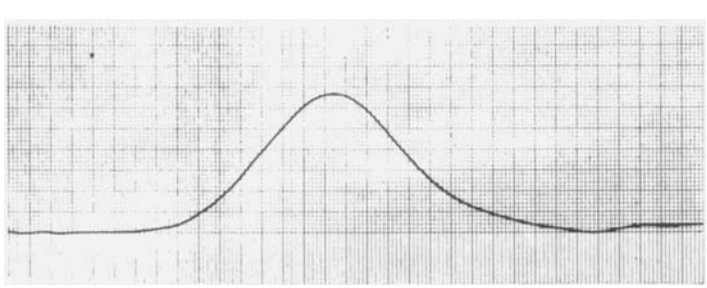

FIGURE 7. A typical temporal record of a soliton wave form as measured by the hot-film probe ($\alpha d = 6{\cdot}96$).

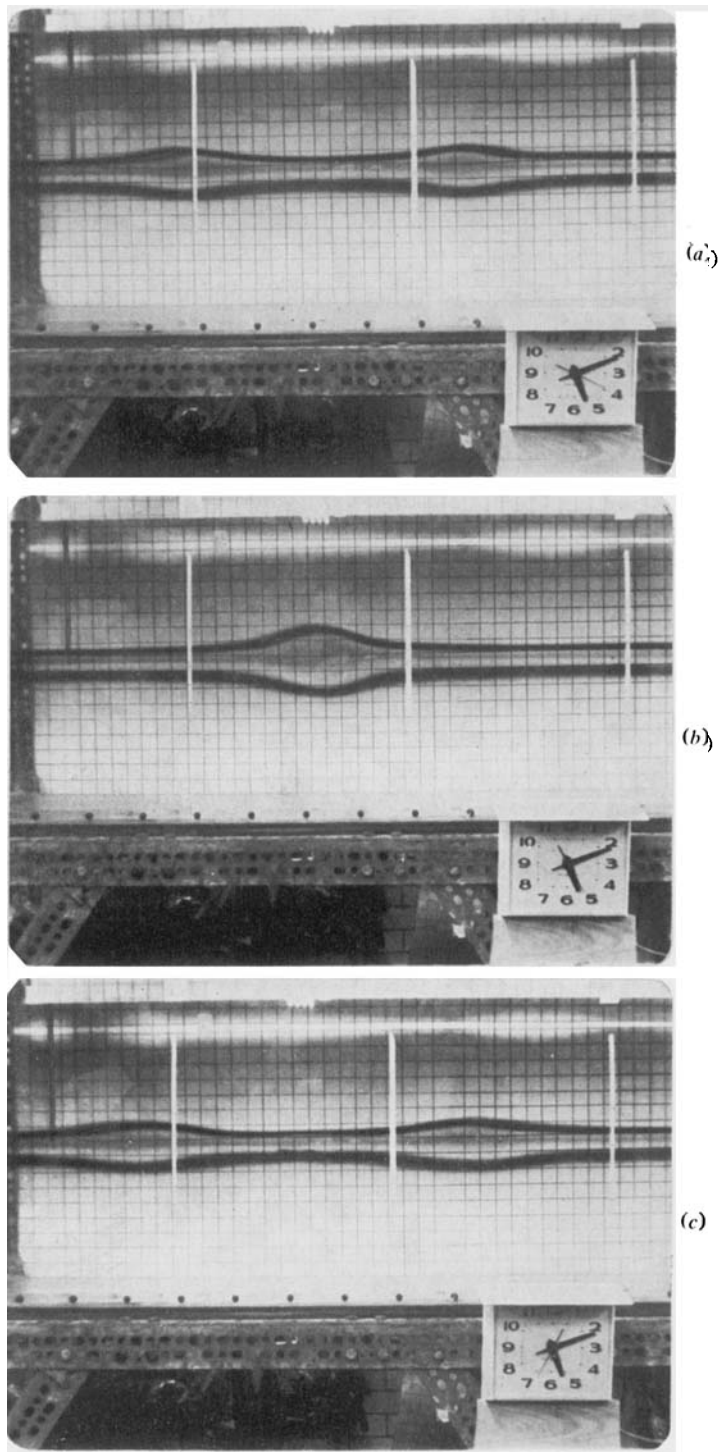

FIGURE 10. A typical visual collision sequence. (*a*) Approximately six seconds before collision. (*b*) Approximately at mid-collision. (*c*) Approximately nine seconds after collision.